ELSEVIER

Journal of Molecular Catalysis A: Chemical 186 (2002) 25–32

JOURNAL OF MOLECULAR CATALYSIS A: CHEMICAL

www.elsevier.com/locate/molcata

Dimanganese(II)-catalase-like model complexes: synthesis, structure characterization and catalytic mechanism

Jian Gao*, Shun He Zhong

College of Chemical Engineering and Technology, Tianjin University, Tianjin 300072, PR China

Received 8 June 2001; received in revised form 11 December 2001; accepted 11 December 2001

Abstract

Synthesis, structure and ESR study of binuclear manganese(II) complexes, which functionally mimic the Mn-catalase enzyme, have been investigated. These complexes are formulated as $[NAPH\,Mn_2\,(\mu\text{-}X)(phen)_2]ClO_4$, (NAPH = 1,8-naphthalate dianion, X = OAc^- (***1***), Cl^-(**2**) and Br^-(**3**)). IR, elemental analyses and electronic spectra, indicated that these complexes have extended bridged structures with both DPHA and μ-X as bridging ligands. The temperature dependence of magnetic susceptibilities of **1** has been studied, giving the exchange integral of $J = -28\,cm^{-1}$, $g = 1.98$. This result is in agreement with the carboxylate group bridged dimanganese structure. Complex **1** was found to be the most active compound for dismutation of H_2O_2 in aqueous solution in which μ-OAC ligand appears to undergo ligand substitution with H_2O molecules. The observed steady-state molecularities for complex **1** presented that the reaction rate is first order with respect to [complex **1**] and zero order with respect to $[H_2O_2]$. Spectroscopic studies support a mechanism involving a Mn_2(III,III) intermediate, which was isolated and verified by IR and element analysis. As a result, a new catalytic mechanism of H_2O_2 dismutation by this complex system was proposed.

Keywords: Dimanganese(II) complexes; Hydrogen peroxide; Catalytic mechanism; Catalase-like activity

1. Introduction

Multinuclear manganese active sites that are vital to biological systems are being steadily recognized and studied. Recently, a number of manganese containing nonhame catalase have been isolated and characterized [1–3]. These enzymes can dismute hydrogen peroxide, a reaction that is important for cell detoxification and a variety of pathological consequences such as aging, diabetes and cancer [4]. Evidence has accumulated that the active sites of the pseudo-catalase isolated from *Lactobacillus plantrum* comprise dinuclear structure per protein subunit [3]. Currently intense efforts have been made to design and synthesize different types of Mn-catalase mimetic complex systems [5–14].

Spectroscopic studies of the dimanganese-catalase enzyme [15,16] have revealed that a "reduced" Mn_2(II, II) state and an "oxidized" Mn_2(III, III) state were implicated in the reaction (Scheme 1) [17]. Whereas, mixed valence state Mn_2(II, III) and Mn_2(III, IV) appear not to be involved. In this work, we report a novel synthetic Mn(II)-catalase model system of high catalase rate. A thorough investigation of the

* Corresponding author. Tel.: +1-979-845-2232; fax: +1-979-845-4719.
E-mail address: gao@mail.chem.tamu.edu (J. Gao).

1381-1169/02/$ – see front matter
PII: S1381-1169(02)00081-X

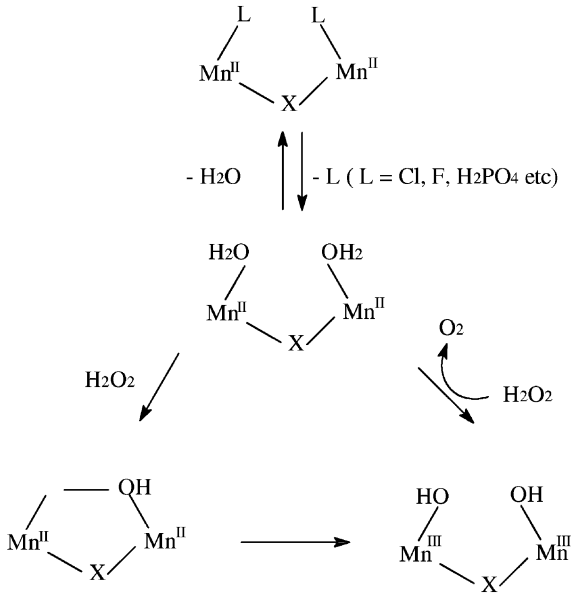

Scheme 1.

structure–activity relationship and the oxidation state preference are described.

2. Experimental

All reagents used are of analytical grade and purchased from Aldrich.

2.1. Preparation of [NAPH Mn_2 (μ-OAc)(phen)$_2$]ClO_4 (1)

In dinitrogen-flushed methanol solution (10 ml) containing 1,8-naphthalic acid (43.2 mg, 0.2 mmol), phen (79.3 mg, 0.4 mmol) and triethylamine (0.4 mmol), a solution of Mn $(ClO_4)_2 \cdot 6H_2O$ (144.8 mg 0.4 mmol) in methanol (15 ml) was added and kept under magnetic stirring; a colorless solution and a few white micro-crystals were obtained. To this mixture was added sodium acetate (0.2 mmol) and yellow precipitates were obtained. The solid product was washed with absolute methanol and diethyl ether three times and dried in *vacuum*. Anal. (%) calcd. for $C_{38}H_{25}O_{10}N_4ClMn_2$, formula weight 843.0: C, 54.1; H, 3.0; N, 6.6; Mn,13.0; found: C, 53.9; H, 3.2; N, 6.8; Mn, 12.5.

2.2. Preparation of [NAPH Mn_2 (μ-Cl)(phen)$_2$] ClO_4 (2)

A similar reaction procedure was followed as stated in above, by using NaCl instead of NaOAc. Yellow microcrystals were obtained. Anal. (%) calcd. for $C_{36}H_{22}N_4O_8Cl_2Mn_2$ formula weight 819.4: C, 52.8; H, 2.0; N, 6.8; Mn, 13.4; found: C, 52.5; H, 2.2; N, 6.6; Mn, 13.2.

2.3. Preparation of [NAPH Mn_2 (μ-Br)$_2$(phen)$_2 \cdot 4H_2O$] (3)

This complex was prepared by following a similar reaction procedure as stated in the previous section by using NaBr instead of NaOAc. Deep-yellow microcrystals were obtained. Anal. (%) calcd. for $C_{36}H_{22}N_4O_8BrClMn_2$, formula weight 863.7: C, 50.0; H, 2.6; N, 6.5; Mn, 12.7; found: C, 50.1; H, 2.9; N, 6.8; Mn, 12.4.

2.4. Measurement

Analysis for C, H, and N was carried out on a Perkin-Elmer analyzer, Model 240 and metal contents were determined by EDTA titration. IR spectra were recorded with a Perkin-Elmer IR spectrophotometer, Model 983G, using KBr-disks, Electronic spectra (in methanol) were measured on a Shimadzu UV-240 spectrophtometer. Solution electrical conductivity measurements were made with a DDS-11A conductometer, Variable-temperature magnetic susceptibilities were measured on a SQUID susceptometer (sensitivity $m = 10^{-6}$ emu). Diamagnetic correction were made with Pascal's constants for all the constituent atoms, and the magnetic moment were calculated using $\mu_{\text{eff}} = 2.828(\chi_M T)^{1/2}$. The ESR spectra were measured with a modified JES-FEIXG by using X-band.

2.5. Study of catalase-like activity

All reactions were carried out at 20 °C and in a 50 ml reactor containing a stirring bar under air. To H_2O (14.7 ml) was added the complex (5 mmol) and the flask was closed with a rubber septum. Hydrogen peroxide (2.7 mmol, 0.3 ml) was injected through the septum with a syringe. The reactor was connected

to a graduated burette filled with water and dioxygen evolution was measured at time intervals during 1 min by volumetry. Observed initial rates were expressed as mol l^{-1} s^{-1} by taking the volume of the solution (15 ml) into account, and calculated from the maximum slope of curve describing evolution of O_2 versus time. In the kinetic study, the total volume (15 ml) was kept unchanged but the concentration of H_2O_2 and the complex catalyst were varied accordingly.

3. Results

3.1. Composition and IR spectroscopic characterization

Satisfactory elemental analyses data were obtained for all these complexes. Molar conductance values fall in the expected range for 1:1 types of electrolyte [18]. (Table 1).

IR spectra for complexes **1**–**3** exhibited two characteristic bands in the 1600–1300 cm^{-1} region, which were attributed to the $|\nu_{as}(COO^-)$ and $\nu_s(COO^-)|$ stretching vibration of the carboxylate groups of NAPH. The separation between ν_{as} and ν_s for these complexes are all smaller than 200 cm^{-1}, suggesting a bidentate mode for both carboxylate groups [19]. For these complexes, intensive CLO_4^- vibrations at 1095 and 620 cm^{-1} were observed, which is typical for non-coordination perchlorate ion [20]. All these data are consistent with the molar conductance measurement.

3.2. Visible absorption spectra of the Mn(II)–Mn(II) complexes

The electronic spectrum of complex **1** was given in Fig. 1. In visible range, no characteristic band was discovered. This phenomenon can easily be interpreted in terms of ligand field theory. For high spin Mn(II)–Mn(II) complex, the ground term is the orbital singlet ^6S. It cannot be split by a crystal field of any symmetry. At high energy region intense bands at ca. 265 and 226 nm were observed, which can be ascribed to "ligand to metal charge transfer" (LMCT). Based on the discussion above, complexes **1**–**3** are proposed to have μ-X bridged dinuclear structure with NAPH as a supporting fragment (Fig. 2).

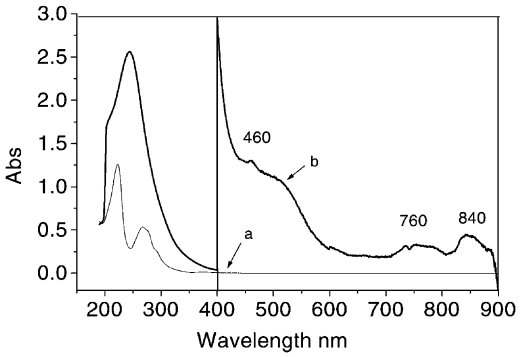

Fig. 1. Electronic spectra of complexes **1** (a) and resulted solution with H_2O_2 stoichiometrically.

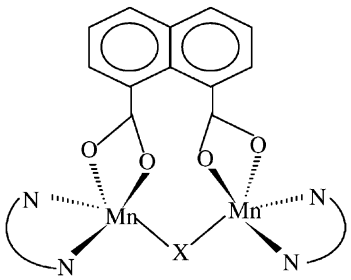

Fig. 2. Proposed structures of these complexes **1**–**3**.

Table 1
Physical and chemical data for complexes **1**–**3**

Complex	Λ_M (Ω^{-1} cm^2 mol^{-1}) in MeCN	IR (cm^{-1})		UV ($\times 10^3$ cm^{-1})	CT	λ_{max} (nm)	ε (M^{-1} cm^{-1})
		$\nu_{as}(COO^-)$	$\nu_s(COO^-)$				
1	132	1570	1430	225	85000	265	34000
2	144	1580	1430	225.6	7800	268	40000
3	160	1560	1420	230	46000	268	16000

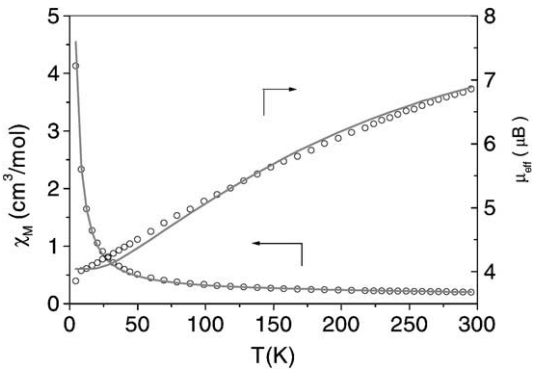

Fig. 3. Temperature variation of magnetic moment of complex **1**.

3.3. Magnetic properties and magnetic structural correlations

Variable-temperature magnetic susceptibility data was collected in the 4.2–300 K ranges. The M versus T plot was shown in Fig. 3. The magnetic moments decrease with decreasing temperature, implying the existence of an antiferromagnetically coupling of Mn(II)–Mn(II) pairs.

Magnetic analysis was carried out based on the Heisenberg spin-exchange operator $H = -JS_1S_2$. The molar susceptibility of the Mn–Mn ($S_1 = S_2 = 5/2$) system was calculated from the equation [21].

$$\chi_M = \frac{2Ng^2\beta^2}{kT}\frac{A}{B}(1-\rho) + \frac{4.37}{T}\rho + N_\alpha,$$

$$A = 55 + 30\exp\left(-10\frac{J}{kT}\right) + 14\exp\left(-18\frac{J}{kT}\right) + 5\exp\left(-24\frac{J}{kT}\right) + \exp\left(-28\frac{J}{kT}\right),$$

$$B = 11 + 9\exp\left(-10\frac{J}{kT}\right) + 7\exp\left(-18\frac{j}{kT}\right) + 5\exp\left(-24\frac{J}{kT}\right) + 3\exp\left(-28\frac{J}{kT}\right) + \exp\left(-30\frac{J}{kT}\right)$$

where χ_M denotes the susceptibility per binuclear complex, N_α the temperature-independent paramagnetism ($120 \times 10^{-6}\,cm^3\,mol^{-1}$), ρ the fraction of mononuclear paramagnetic impurity, and other symbols have their usual meaning. As shown in Fig. 3, good fit to the experimental data were attained. The magnetic parameters thus determined are $J = -28\,cm^{-1}$, $g = 1.99$, $\rho = 0.005$. This result indicated that μ-OAc bridged dinuclear complexes undergo intermediate spin-coupling between the adjacent metal ions [22], and it is a little higher than related μ-OAc bridged Mn(II)–Mn(II) complexes [7,23]. The quantitative difference of the spin-coupling between complex **1** and other NAPH bridged dinuclear complexes [22,24] is easy to illustrate. As spin interaction caused by NAPH is less than $-5\,cm^{-1}$, the increased anti-ferromagnetic interaction was due to the introduction of μ-OAc bridge

3.4. Catalytic activity of complexes *1*–*3*

As these complexes are soluble in water, the reaction was easily carried out in homogeneous condition. The catalase-like activity was tested by measuring the dioxygen evolution with a Mn_2 complex:H_2O_2 ratio of 1:500 and a catalyst concentration of 0.4 mmol/l. These conditions were found to be optimal in terms of reaction rate. The amount of residual hydrogen peroxide (measured by iodometric titration) was compared with the amount of dioxygen formed and was found to satisfy the stoichiometry implied by Eq. (1):

$$2H_2O_2 \rightarrow 2H_2O + O_2 \quad (1)$$

The time courses of oxygen evolution for these complexes were given in Fig. 4. For complex **1**, the rapid dioxygen evolution rate was reached after the reaction was initiated and slowed down as the reaction proceeded. When the catalytic process ceased, the evolved

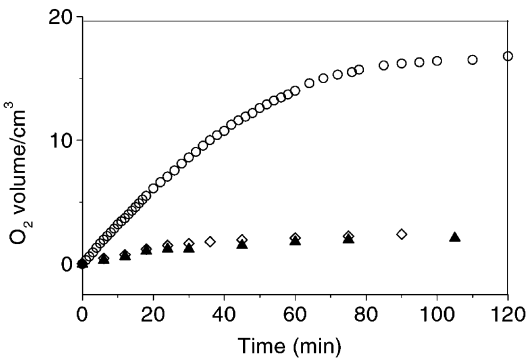

Fig. 4. Time course of oxygen evolution in the disproportionation of H_2O_2 by complexes **1** (○), **2** (◇) and **3** (▲); the concentration of the complexes were 4.0×10^{-4}; $[H_2O_2] = 1.76 \times 10^{-1}$ M.

Table 2
Reaction rates for disproportionation of H_2O_2 by complexes **1**–**3**

Complex	Rate (mol dm^{-3} s)
1	1.5×10^{-5}
2	2.4×10^{-6}
3	2.0×10^{-6}

dioxygen gas corresponds to 100% decomposition of hydrogen peroxide. No lag phase was observed at the initial stage. Complexes **2** and **3** showed the similar evolution profiles, however, at relatively low reaction rates. The observed initial rates for these complexes were compiled in Table 2.

3.5. Reactant molecularity

The steady rate of O_2 evolving was found to be first order in complex **1** and zero order in hydrogen peroxide. Fig. 5 shows a plot of the dependence of the rate on the concentration of complex **1** with the concentration of H_2O_2 is held constant. Fig. 6 presents the dependence of the steady-state rate on the concentration of H_2O_2. This result is different from related model systems [25,26]. The average k_{obs} obtained is equal to 3.80×10^{-2} s^{-1}.

3.6. Water as reactant

Addition of a percentage of methanol to an aqueous solution of complex **1** prior to addition of

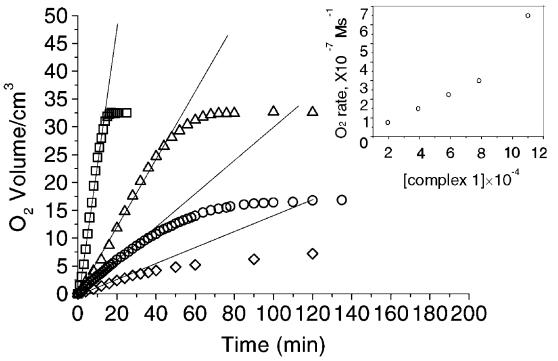

Fig. 5. The rate of H_2O_2 formation at constant H_2O_2 ($[H_2O_2] = 1.76 \times 10^{-1}$ M) concentration and different concentration of complex **1** (for (◇), (○), (△), and (□) the Cu_2 concentration are 2.0×10^{-4}, 4.0×10^{-4}, 6.0×10^{-4} and 8.0×10^{-4} M, respectively).

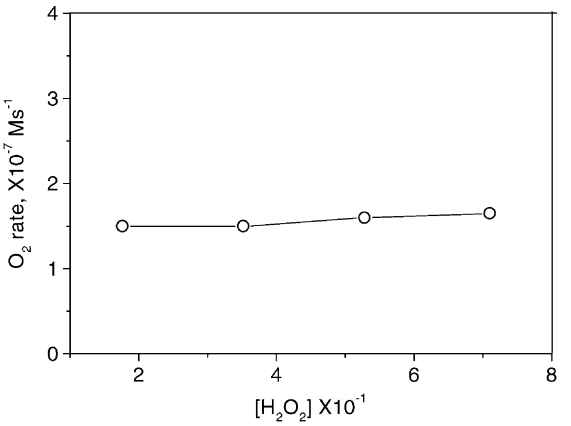

Fig. 6. The rate of O_2 formation as a function of H_2O_2 at constant concentration of complex **1**: [complex ***1***] $= 3.92 \times 10^{-4}$ M.

H_2O_2 increase the initial lag phase and decrease the steady-state rate. By holding the concentration of H_2O_2 and **1** constant, the rate of O_2 production was measured as a function of water concentration (Fig. 7). The steady rate at which O_2 is produced decreased as the water concentration was decreased. The initial lag time for O_2 production increases to 5 min when the percentage of water was almost zero.

3.7. Labile μ-OAC ligand

For these three complexes, the only difference is the type of μ-X ligand. As observed, μ-OAC complex

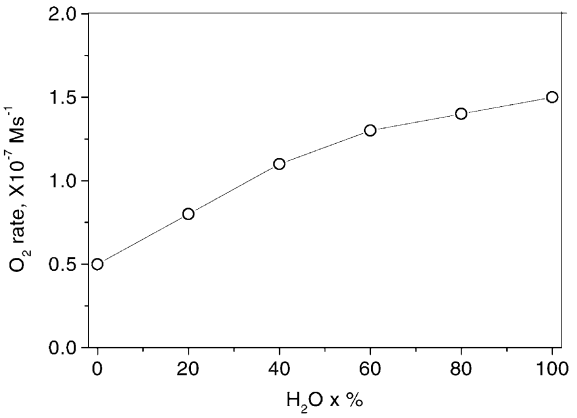

Fig. 7. The rate of O_2 formation as a function of percentage of water: [complex ***1***] $= 3.92 \times 10^{-4}$; $[H_2O_2] = 1.76 \times 10^{-1}$ M.

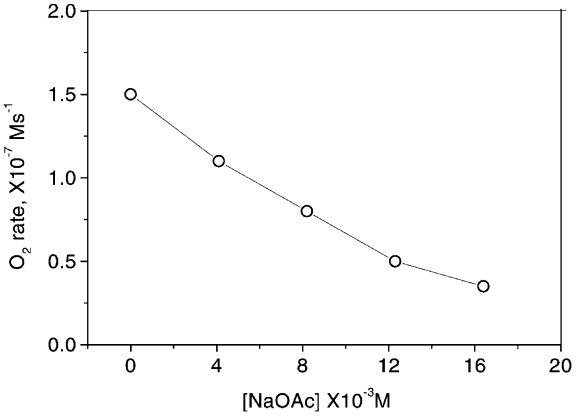

Fig. 8. The rate of O_2 formation as a function of NAOAc concentration: [complex ***1***] $= 3.92 \times 10^{-4}$; $[H_2O_2] = 1.76 \times 10^{-1}$ M.

is more active than those of Cl and Br. This result indicated that OAC is substitution-labile comparing to Cl and Br [27]. As an extensive study, sodium acetate was used to testify the exchanging behavior of μ-OAC ligand. As shown in Fig. 8, addition of NaOAc to the aqueous reaction mixture caused the decrease of the reaction rate of O_2.

3.8. Catalytic intermediates

The reaction complex **1** with a stoichiometric amount of H_2O_2 produced a yellow colored solution

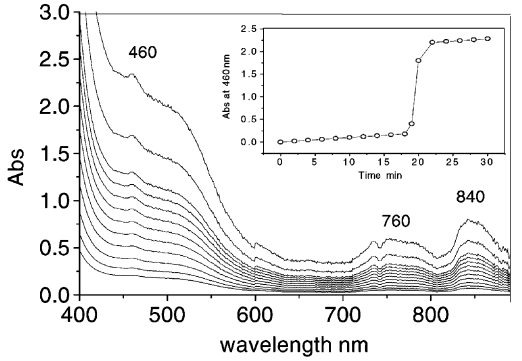

Fig. 10. Time dependence of visible spectral changes in the catalytic reaction with complex **1**.

having visible-range spectra shown in Fig. 1. Peaks at 460, 760 and 840 nm indicated that Mn(III) or Mn_2(III, III) species are formed in the reaction [28]. IR spectrum of the final complex exhibits three additional bands at 640, 580 and 520 cm^{-1} (Fig. 9). These featured bands were assigned to Mn_2(III, III) (μ-O) or Mn(III) related species [29].

Fig. 10 shows the time dependence of absorbance monitored at 460 nm, which is characteristic of Mn(III). The catalytic intermediates were also studied by ESR technique. The reaction was performed in aqueous solution and the low-temperature ESR spectroscopy was monitored freezing in liquid nitrogen. In the catalytic reaction, as the color-less solution

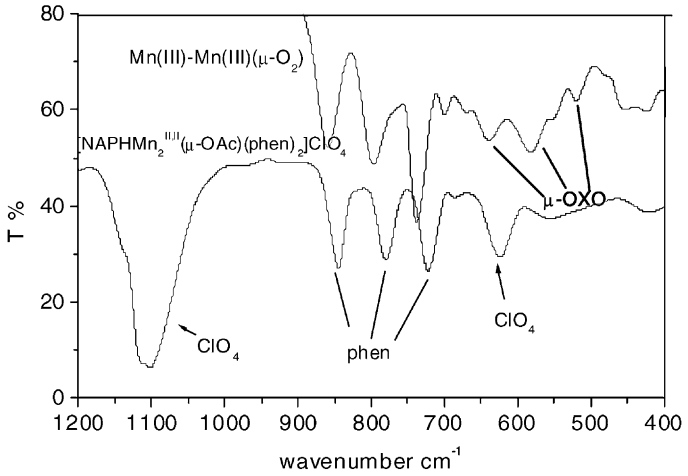

Fig. 9. IR spectrum of intermediate complex Mn_2(III, III) (μ-O).

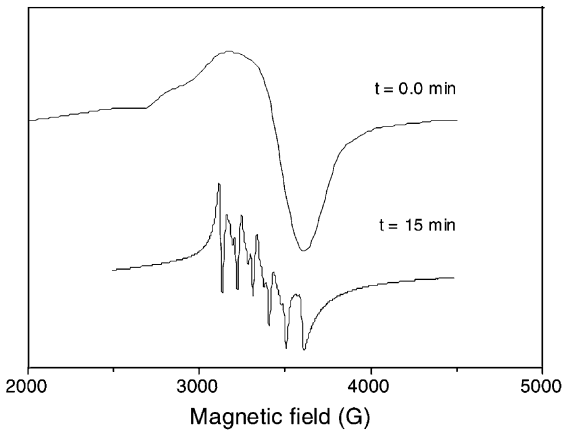

Fig. 11. The reaction of complex **1** with H_2O_2 monitored by ESR.

turned to yellow, the dramatic change was observed in the ESR spectra (Fig. 11). Once the reaction reached steady-state in 15 min, there is a 60% decrease in the Mn_2(II, II) ESR signal intensity. As a minor amount of uncoupled high symmetry Mn^{2+} species formed, the six-line ESR signal was observed. This phenomenon indicated that the ESR silent Mn(III)–Mn(III) species co-exist with Mn^{2+} mononuclear species in the solution. The concurrence of these two phenomenon suggests that the oxidation of Mn(II)–Mn(II) center by hydrogen peroxide is closely related with the catalase-like function of the complex.

4. Discussion

The initial stage for complex **1** catalyzed reaction involves a equilibrium with water, possibly by dissociation of μ-OAC as shown by Figs. 7 and 8. These data are evidence for the first step of proposed mechanism (Scheme 2). The active form of [NAPHMn$_2$(II, II)(H_2O)(phen)$_2$] favors the binding of hydrogen peroxide to the Mn(II)–Mn(II) center by displacing of the bound water in step (2). Thus, a dioxygen

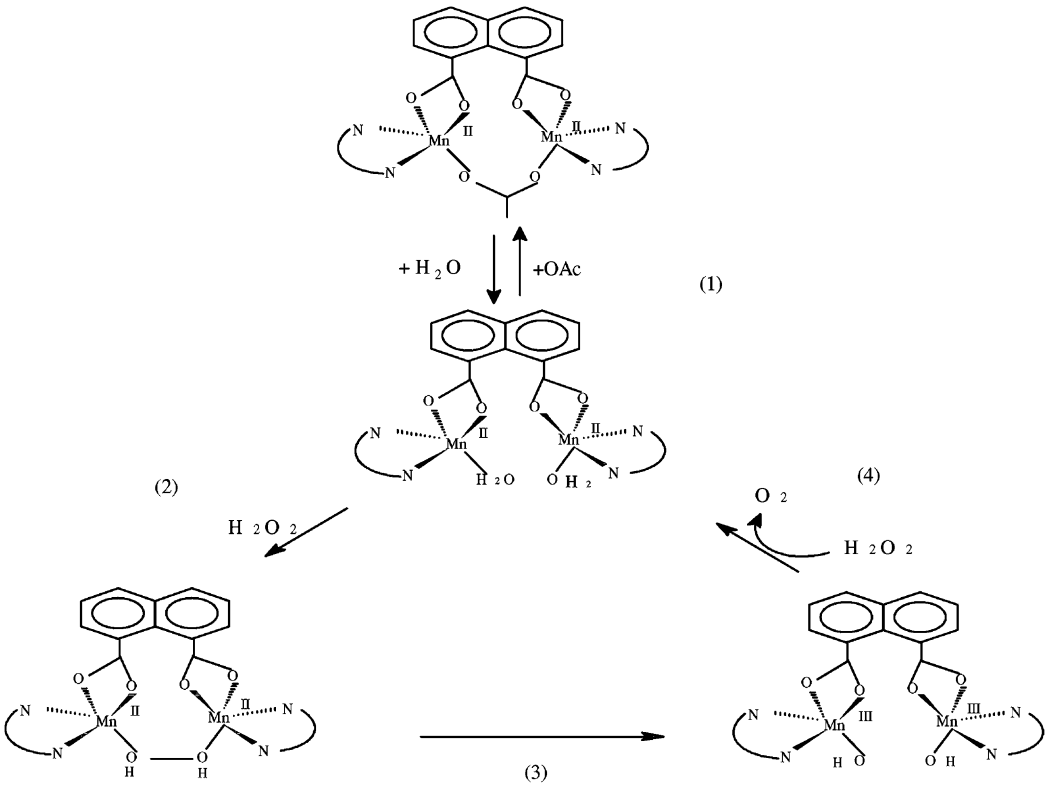

Scheme 2.

adduct Mn(III)–O_2–Mn(III) formed. Electronic absorption spectra in Fig. 10 and ESR profiles of Fig. 11 support the formation of a ESR silent Mn(III)–Mn(III) intermediate. Hence, in step (3), intermolecular electronic transfer occurred in which Mn(II) ions were oxidized to Mn(III) ions, concurrent with reduction of peroxide. Subsequently, Mn(III) ions were reduced by a second H_2O_2 molecule. At this stage the complex catalyst was restored to its initial active form.

References

[1] Y. Kono, I. Fridovich, J. Biol. Chem. 258 (1983) 6015.
[2] G.S. Algood, J.J. Perry, J. Bacteriol. 168 (1986) 563.
[3] V.V. Barynin, A. Grebenko, Dokl. Akad. Nauk. S.S.S.R. 286 (1986) 461.
[4] O. Hayaish, E. Niki, M. Kondo, Yoshikawa (Eds.), Medical, Biochemical and Chemical Aspects of Free Radicals, Elsevier, Amsterdam, 1990.
[5] H. Sakiyama, H. Okawa, M. Suzuki, Chem. Soc., Dalton Trans. (1993) 3823.
[6] H. Sakiyama, H. Okawa, M. Suzuki, Chem. Soc., Chem. Commun. (1993) 882.
[7] C. Higuchi, H. Sakiyama, H. Okawa, R. Isobe, D.E. Fenton, J. Chem. Soc., Dalton. Trans. (1994) 1097.
[8] T. Nagata, Y. Ikawa, K. Maruyama, J. Chem. Soc., Chem. Commun. (1994) 471.
[9] Y. Naruta, K. Maruyama, J. Am. Chem. Soc. 113 (1991) 3595.
[10] Y. Naruta, M. Sasayama, J. Chem. Soc., Chem. Commun. (1994) 2667.
[11] U. Bossek, M. Saher, T. Weghermuller, K. Wieghardt, J. Chem. Soc., Chem. Commun. (1992) 1780.
[12] E.J. Larson, V.L. Pecoraro, J. Am. Chem. Soc. 113 (1991) 7809.
[13] E.J. Larson, V.L. Pecoraro, J. Am. Chem. Soc. 113 (1991) 3810.
[14] P. Mathur, M. Crowder, G.C. Dismukes, J. Am. Soc. 109 (1987) 5227.
[15] S.V. Khangulov, M.G. Goldfeld, V.V. Gerasimenko, N.E. Andreeva, V.V. Barynin, A.I. Grebenko, J. Inorg. Biochem. 40 (1990) 279.
[16] G.S. Waldo, S. Yu, J.E.P. Hahn, J. Am. Chem. Soc. 114 (1992) 5869.
[17] G.C. Dismukes, Polynuclear manganese enzymes, in: J. Reedijk (Ed.), Bioinorganic Catalysis, Marcel Dekker, Amsterdam, 1992.
[18] W.J. Geary, Coord. Chem. Rev. 7 (1971) 81.
[19] E. Bakalbassis, J. Gouterou, S. Jeannin, Y. Jeannin, Kahn, Inorg. Chem. 32 (1993) 2056.
[20] M.R. Rosenthal, J. Chem. Edu. 50 (1973) 331.
[21] D. Luneau, J.M. Savariault, P. Cassoux, J.P. Touchagues, J. Chem. Soc., Dalton Trans. (1988) 1225.
[22] J. Gao, Polish J. Chem. 72 (1998) 839.
[23] M. Yamami, M. Tanaka, H. Sakiyama, T. Koja, K. Kobayashi, H. Miyasaka, M. Ohba, H. Okawa, J. Chem. Soc., Dalton Trans. (1997) 4595.
[24] J. Gao, Polish J. Chem. 72 (1998) 695.
[25] C. Higuchi, H. Sakiyama, H. Okawa, D.E. Fento, J. Chem. Soc., Dalton Trans. (1995) 4015.
[26] P.J. Pessiki, G.C. Dismukes, J. Am. Chem. Soc. 116 (1994) 898.
[27] S. Menage, J.M. Vincent, C. Lambeaux, M. Fontecave, J. Chem. Soc., Dalton Trans. (1994) 2081.
[28] J.E. Sheats, R. Czernuziewicz, G.C. Dismukes, A. Rheingold, V. Petronleas, J. Stubbe, W.H. Armstrong, R. Beer, S.J. Lippard, J. Am. Chem. Soc. 109 (1987) 1435.
[29] K. Wieghardt, U. Bossek, J. Bonvoism, P. Beanvillain, J.J. Girerd, B. Nuber, J. Weiss, J. Heinze, J. Angew. Chem. Int. Ed. Engl. 25 (1986) 1030.